# Supporting Information

# Synthesis and Study of the First Zeolitic Uranium Borate

Yucheng Hao[†], Vladislav V. Klepov[§], Philip Kegler[†], Giuseppe Modolo[†], Dirk Bosbach[†], Thomas E. Albrecht-Schmitt[ξ], Shuao Wang[Δ] and Evgeny V. Alekseev[†,‡,*]

[†]Institute of Energy and Climate Research (IEK-6), Forschungszentrum Jülich GmbH, 52428 Jülich, Germany

[‡]Institut für Kristallographie, RWTH Aachen University, 52066 Aachen, Germany

[§]Department of Chemistry, Samara National Research University, 443086 Samara, Russia

[ξ]FSU Department of Chemistry and Biochemistry, Florida State University, 95 Chieftan Way, Tallahassee, FL 32306-4390, United States of America

[Δ]School for Radiological and Interdisciplinary Sciences (RAD-X) and Collaborative Innovation Center of Radiation Medicine of Jiangsu Higher Education Institutions, Soochow University, Suzhou 215123, China

*contact E-Mail: e.alekseev@fz-juelich.de*

**Figure S6.** (a) A regular hexagon B-ring in **LUBO**, (b) an irregular hexagon B-ring in $PbB_4O_7$.

**Figure S7.** Coordination types of uranyl group in the compound of **LUBO**. (a)View of the local coordination environment around a uranium center atom; (b) a view of the uranyl bipyramids in the 3D boron framework structure of **LUBO** along *c*-axis.

**Figure S8**. A new 4-nodal net topological type with a Schläfli symbol of $\{3^3.4^3.6^2.7^2\}_6\{3^4.4^3.5^2.6\}_6$ $\{3^4.4^6.5^4.6^6.7^4.8^4\}_3\{4^3\}_2$. Uranium and boron are shown as yellow and green nodes.

**Figure S9**. Coordination type of uranyl group in the compound of $Li[(UO_2)B_5O_9](H_2O)$. (a)View of the local coordination environment around a uranium center atom; (b) a view of the uranyl hexagonal bipyramids in the 3D framework structure along *b*-axis.

**Figure S10**. The oxygen coordination environment around the Pb atom (a); Voronoi-Dirichlet polyhedron of the Pb atom in the structure of **LUBO** (b).

**Figure. S11**. Construction of the anionic borate framework using natural tiling. (a) A new $[3^6\bullet6^2\bullet8^3]$ CBU cage; (b) the connectivity mode of the CBUs with other tiles; (c-e) the tiling structure of LUBO viewed along *a*, *c*, *b*-axis, tile faces partly omitted for clarity of tunnels; (f) illustration of the channel system and cavities in PbUBO by tiles. (g) a $[6^3]$ *t-kah* unit; (h) a new larger cage $[3^6\bullet6^3\bullet8^9]$.

**Figure S12.** The underlying topology and tiling of borate framework $[(B_{14}O_{27})^{12-}]$ based on the $[3^66^28^3]$ CBU. (a) The underlying topology is the six coordinated net, the centers of the $[3^66^28^3]$ CBUs fall on the nodes (red ball). The connections of the boron in the net are shown in grey. (b) The channels of $[(B_{14}O_{27})^{12-}]$ represented by two types of tiles; $[3^66^28^3]$ and $[3^66^38^9]$ cages.

**Figure S13**. The three different tiles in the borate framework of **LUBO**.The face symbles are on top and V, E, F ( number of (vertices, edges and faces) on the bottom of the tiles.

**Figure S14**. Plotting of TG-DSC curves of **LUBO**.

**Table S1**. Important Bond lengths (Å) and angles (°) for **LUBO**.

| | | | | | |
|---|---|---|---|---|---|
| U(1)=O(6)#1 | 1.793(10) | U(1)=O(6) | 1.793(10) | U(1)-O(4)#1 | 2.358(8) |
| U(1)-O(4) | 2.358(8) | U(1)-O(3)#1 | 2.479(9) | U(1)-O(3) | 2.479(9) |
| U(1)-O(2)#1 | 2.521(8) | U(1)-O(2) | 2.521(8) | | |
| | | | | | |
| Pb(1)-O(5) | 2.426(9) | Pb(1)-O(5)#2 | 2.426(9) | Pb(1)-O(1) | 2.514(12) |
| | | | | | |
| O(3)-B(1) | 1.483(16) | B(1)-O(4)#1 | 1.480(15) | B(1)-O(5) | 1.467(16) |
| B(1)-O(5)#6 | 1.469(15) | B(2)-O(1)#3 | 1.467(14) | B(2)-O(1)#4 | 1.467(14) |
| B(2)-O(2) | 1.509(15) | B(2)-O(3) | 1.473(14) | B(2)-O(4)#5 | 1.452(15) |
| B(3)-O(2)#5 | 1.371(8) | B(3)-O(2)#8 | 1.371(8) | B(3)-O(2) | 1.371(8) |

| | | | |
|---|---|---|---|
| O(6)#1-U(1)-O(6) | 180.0(5) | O(4)-U(1)-O(4)#1 | 180.000(1) |
| O(3)-U(1)-O(3)#1 | 180.000(1) | O(2)-U(1)-O(2)#1 | 180.0(3) |
| | | | |
| O(5)#2-Pb(1)-O(5) | 140.4(4) | O(5)#2-Pb(1)-O(1) | 87.5(2) |
| O(5)-Pb(1)-O(1) | 87.5(2) | | |
| | | | |
| B(2)#3-O(1)-B(2)#4 | 133.4(13) | B(3)-O(2)-B(2) | 126.4(8) |
| B(2)-O(3)-B(1) | 126.5(9) | B(2)#5-O(4)-B(1)#1 | 123.5(9) |
| B(1)-O(5)-B(1)#6 | 119.5(6) | O(5)-B(1)-O(5)#7 | 110.5(11) |
| O(5)-B(1)-O(4)#1 | 111.3(10) | O(5)#7-B(1)-O(4)#1 | 108.6(10) |
| O(5)-B(1)-O(3) | 108.4(11) | O(5)#7-B(1)-O(3) | 114.0(10) |
| O(4)#1-B(1)-O(3) | 103.9(9) | O(4)#8-B(2)-O(1)#9 | 107.5(10) |
| O(4)#8-B(2)-O(3) | 111.1(10) | O(1)#9-B(2)-O(3) | 113.4(10) |
| O(4)#8-B(2)-O(2) | 110.0(9) | O(1)#9-B(2)-O(2) | 113.1(10) |
| O(3)-B(2)-O(2) | 101.6(9) | O(2)#5-B(3)-O(2) | 119.98(6) |
| O(2)#5-B(3)-O(2)#8 | 119.98(6) | O(2)-B(3)-O(2)#8 | 119.98(6) |

Symmetry transformations used to generate equivalent atoms: #1 -x+1, -y+2, -z+1; #2 x, y, -z+3/2; #3 -x+y+1, -x+2, -z+3/2; #4 -x+y+1, -x+2, z; #5 -y+1, x-y+1, z; #6 y, -x+y+1, -z+1; #7 x-y+1, x, -z+1; #8 -x+y, -x+1, z; #9 -y+2, x-y+1, z.

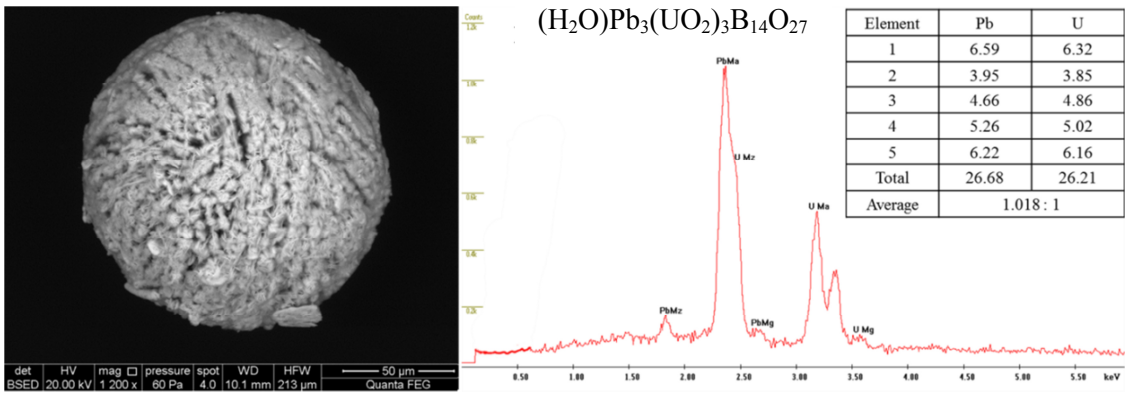


| Element | Pb | U |
|---|---|---|
| 1 | 6.59 | 6.32 |
| 2 | 3.95 | 3.85 |
| 3 | 4.66 | 4.86 |
| 4 | 5.26 | 5.02 |
| 5 | 6.22 | 6.16 |
| Total | 26.68 | 26.21 |
| Average | 1.018 : 1 | |

**Figure S1**. EDS analysis and SEM image for **LUBO**.

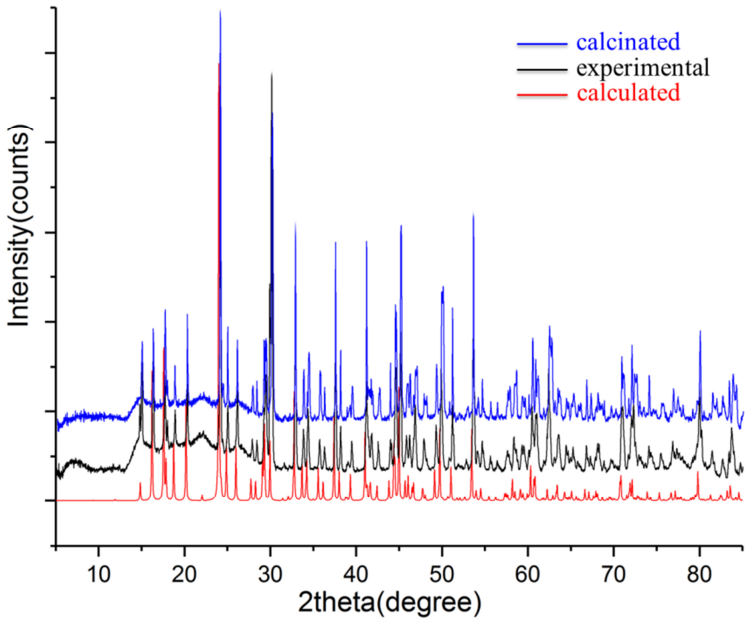


**Figure S2**. Calcinated, experimental and calculated powder X-ray diffraction patterns of **LUBO**.

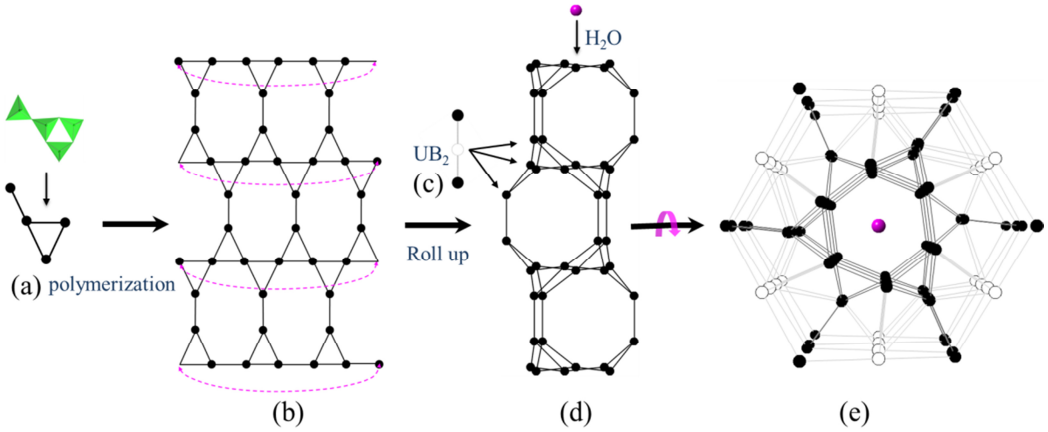


**Figure S3.** A schematic representation of segments hierarchy in **LUBO** hexagonal channels. (a) A fundamental building block (FBB) of the channel; (b) corresponding unfold version of the hexagonal channel cationic topology representation $[(3.8^2)(3^2.8^2)]$; (c) a $[(UO_2)(BO_3)_2]$ cluster topology representation; (d) a hexagonal channel topology representation along the *c*-axis; (e) view of coordinated environments for the hexagonal channel along the *c*-axis.

The formation of the hexagonal channel segment in **LUBO** from cationic topology view is diagrammatically shown in figure S3, S4. The fundamental building block (FBB) of the hexagonal channels is $(B_4O_{13})^{14-}$ ($B_4$) tetramer (see Figure S3a). This fragment is based on four $BO_4$ tetrahedra (4□):<3□>□ according to the borate classification system proposed by Burns[1]. This FBB has been known only in natural uralborite[50], but not found in any other actinide borates up to now.[2, 3, 4] These $B_4$ tetramer groups form via corner-sharing polymerization a quasi 2D layer with the structure shown in figure S4b. The layer has 8-membered holes, which are different with those observed in actinide borates earlier described by Wang and Wu[2, 5]. The hexagonal tunnels are a result of the simple rolling up of the quasi layers (see Figure S3c). The resulting borate hexagonal channels are externally enclosed by $[(UO_2)(BO_3)_2]$ ($UB_2$) clusters *via* edge or corner sharing of uranyl units and corner sharing of $BO_3$ triangles, respectively (see Figure S3d). These $[(UO_2)(BO_3)_2]$ clusters are in alignment with each other along the *c*-axis. They are shifted on 0.5*c* and the angles are 60° between the adjacent groups. This shift has led to a linear shape along the *c*-axis. The resulting complex hexagonal channels have a six-point star

topology. It is a rare borate-based hexagonal channel with a stick shape which is encrusted by $UB_2$ groups outside (see Figure S3e).

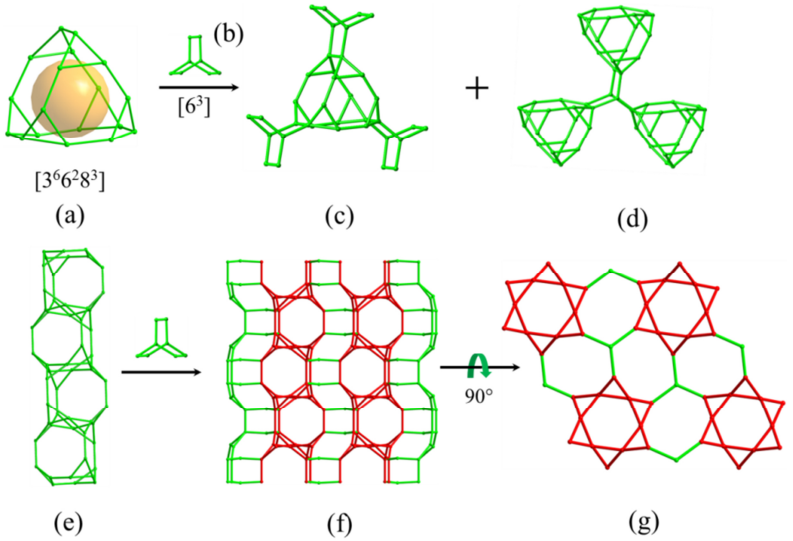


**Figure S4.** Construction of the borate framework $[(B_{14}O_{27})^{12-}]$ under cationic topology view. (a) A new $[3^6 6^2 8^3]$ CBU unit; (b) a three DTs $[6^3]$ unit; (c), (d) the connection modes of $[3^6 6^2 8^3]$ CBU and DTs $[6^3]$ unit. (e) the connection way of $[3^6 6^2 8^3]$ CBU units along *c*-axis; (f), (g) view of the 3D cation network along the *a*, *c*-axis. The boron cations are shown as green, the yellow ball is a model for seeing the cage space clearly.

A clear and precise representation of the borate framework may be given using the description which is usually employed in zeolite structural chemistry. Although zeolite structures usually contains two types of cations, i.e. Al-Si, Al-B, B-Si, B-Ge, Ga-Ge, etc., the borate framework in **LUBO** has only single sort of boron cations. $(B_{14}O_{27})^{12-}$ framework can be considered as built from a novel quasi *d6r* $[3^6 6^2 8^3]$ composite building unit (CBU) shown in Figure S4, which is comparable to Cancrinite structure's $[4^6 6^2 6^3]$ CBU[7]. The face symbols given in the square brackets represent the topology of a CBU. For example, $[3^6 6^2 8^3]$ CBU is a cage containing six triangular faces, two hexagonal, and three octagonal faces. In **LUBO**, each $[3^6 6^2 8^3]$ CBU is connected to six other *via* three double triangles (DTs) $[6^3]$ units (see Figure

4b, c, d) in two directions, defining a layer containing 6- and 8-MRs in the *ab*-plane. The connectivity in the perpendicular direction is achieved by sharing the 6-MR windows by [$3^6 6^2 8^3$] CBUs (see Figure 4e). The simplified 3-nodal net of $(B_{14}O_{27})^{12-}$ framework was attributed to $(3.6.8^4)_3(3^2.6.7^2.8)_3(6^3)$ point symbol (see Figure 4f, 4g and Figure S3).[8-10] The simplified net exhibits all the features of the initial framework, i.e. there are 6- and 8-MRs corresponding to the channels in the initial borate framework.

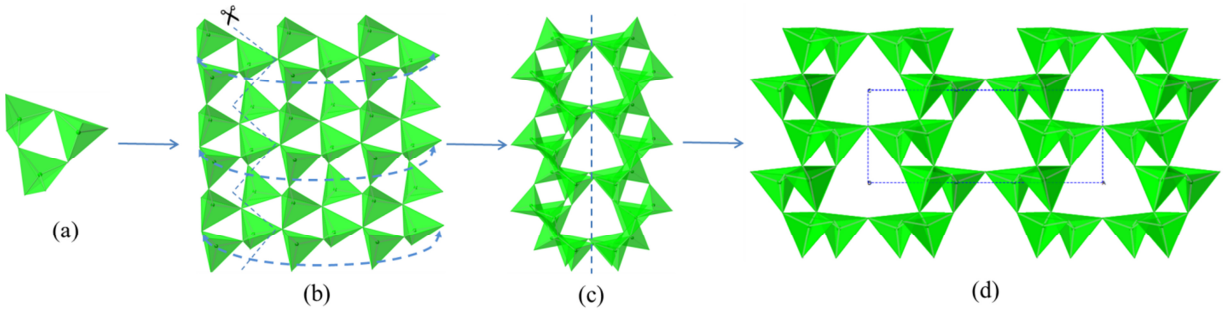


**Figure S5**. The hexagonal channel construction of $PbB_4O_7$.

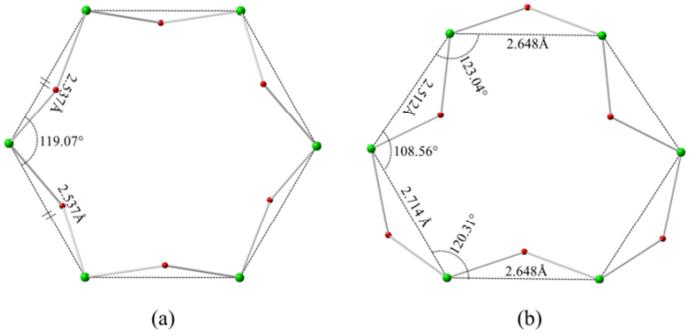


**Figure S6.** (a) A regular hexagon B-ring in **LUBO**, (b) an irregular hexagon B-ring in $PbB_4O_7$.

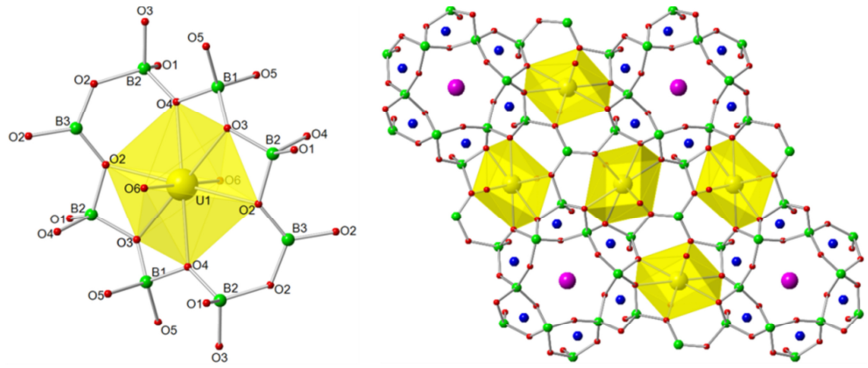


(a) (b)

**Figure S7.** Coordination types of uranyl group in the compound of **LUBO**. (a)View of the local coordination environment around a uranium center atom; (b) a view of the uranyl bipyramids in the 3D boron framework structure of **LUBO** along *c*-axis.

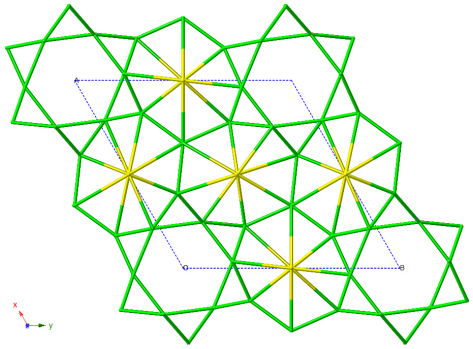

**Figure S8**. A new 4-nodal net topological type with a Schläfli symbol of $\{3^3.4^3.6^2.7^2\}_6\{3^4.4^3.5^2.6\}_6$ $\{3^4.4^6.5^4.6^6.7^4.8^4\}_3\{4^3\}_2$. Uranium and boron are shown as yellow and green nodes.

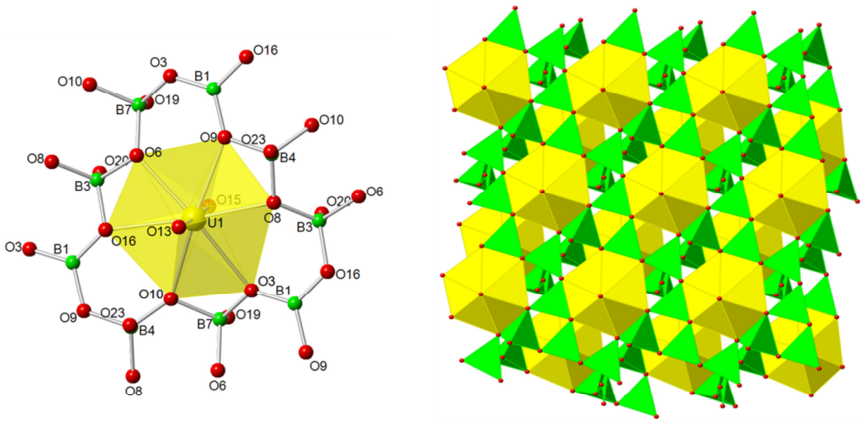


(a) (b)

**Figure S9**. Coordination type of uranyl group in the compound of $Li[(UO_2)B_5O_9](H_2O)$. (a)View of the local coordination environment around a uranium center atom; (b) a view of the uranyl hexagonal bipyramids in the 3D framework structure along *b*-axis.

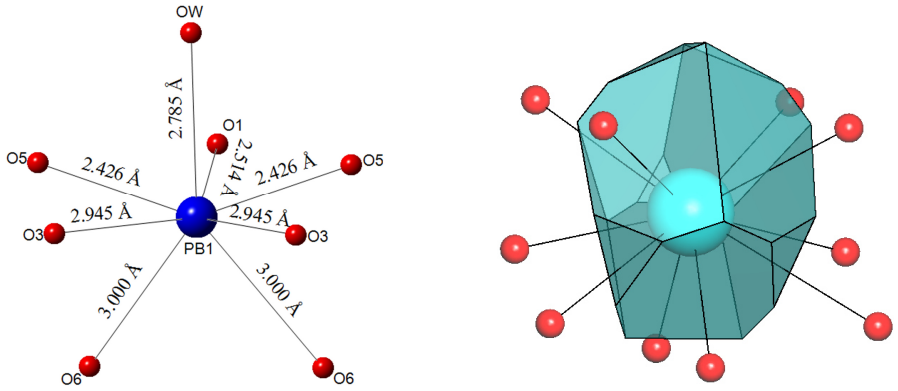


(a) (b)

**Figure S10**. The oxygen coordination environment around the Pb atom (a); Voronoi-Dirichlet polyhedron of the Pb atom in the structure of **LUBO** (b).

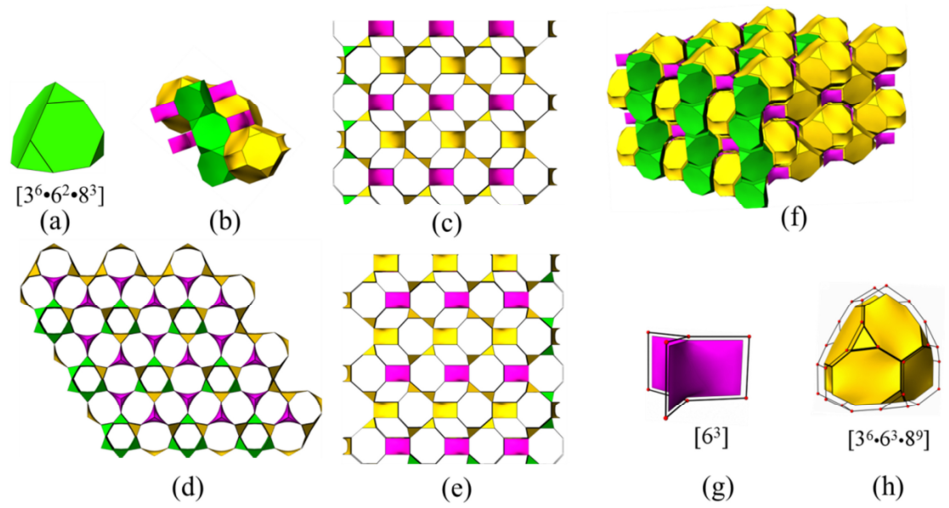


**Figure. S11**. Construction of the anionic borate framework using natural tiling. (a) A new [$3^6$•$6^2$•$8^3$] CBU cage; (b) the connectivity mode of the CBUs with other tiles; (c-e) the tiling structure of LUBO viewed along *a*, *c*, *b*-axis, tile faces partly omitted for clarity of tunnels; (f) illustration of the channel system and cavities in PbUBO by tiles. (g) a [$6^3$] *t-kah* unit; (h) a new larger cage [$3^6$•$6^3$•$8^9$].

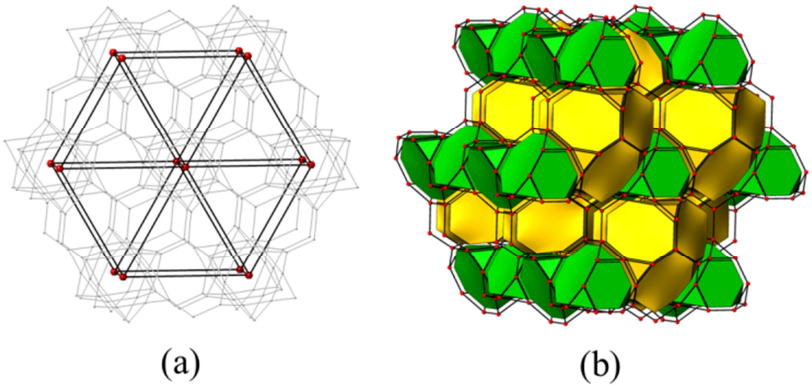


**Figure S12.** The underlying topology and tiling of borate framework [$(B_{14}O_{27})^{12-}$] based on the [$3^6 6^2 8^3$] CBU. (a) The underlying topology is the six coordinated net, the centers of the [$3^6 6^2 8^3$] CBUs fall on the nodes (red ball). The connections of the boron in the net are shown in grey. (b) The channels of [$(B_{14}O_{27})^{12-}$] represented by two types of tiles; [$3^6 6^2 8^3$] and [$3^6 6^3 8^9$] cages.

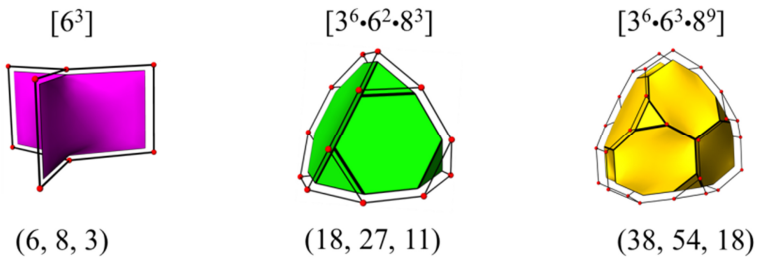


**Figure S13**. The three different tiles in the borate framework of **LUBO**.The face symbles are on top and V, E, F ( number of (vertices, edges and faces) on the bottom of the tiles.

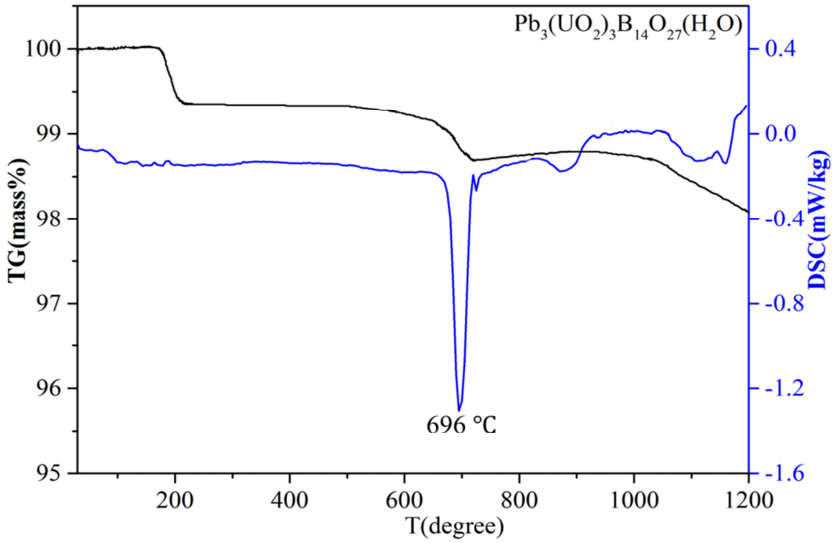


**Figure S14**. Plotting of TG-DSC curves of **LUBO**.

**References:**

(1) Burns, P. C., Borate clusters and fundamental building blocks containing four polyhedra: why few clusters are utilized as fundamental building blocks of structures. *CAN. MINERAL*. **1995**, *33*, 1167.

(2) Kusachi, I., Shiraga, K., Kobayashi, S., Yamakawa, J. and Takechi, Y., Uralborite from Fuka, Okayama Prefecture, Japan. *J MINER PETROL SCI*. **2000**, *95*, 43.

(3) Wang, S., Alekseev, E. V., Depmeier, W. and Albrecht-Schmitt, T. E., Recent progress in actinide borate chemistry. *Chem. Commun*. **2011**, *47*, 10874.

(4) Hao, Y., Klepov, V. V., Murphy, G. L., Modolo, G., Bosbach, D., Albrecht-Schmitt, T. E., Kennedy, B. J., Wang, S. and Alekseev, E. V., Influence of Synthetic Conditions on Chemistry and Structural Properties of Alkaline Earth Uranyl Borates. *Cryst. Growth Des*. **2016**, *16*, 5923.

(5) Xu X., Liu Z., Yang S., Chen L., Diwu J., Alekseev E. V., Chai Z., Albrecht-Schmitt T. E., Wang S. Potassium uranyl borate 3D framework compound resulted from temperature directed hydroborate condensation: structure, spectroscopy, and dissolution studies. *Dalton Trans.*, **2016**, *45*, 15464.

(6) Wu, S., Wang, S., Polinski, M., Beermann, O., Kegler, P., Malcherek, T., Holzheid, A., Depmeier, W., Bosbach, D., Albrecht-Schmitt, T. E. and Alekseev, E. V., High Structural Complexity of Potassium Uranyl Borates Derived from High-Temperature/High-Pressure Reactions. *Inorg. Chem*. **2013**. *52*, 5110.

(7) Dana, E. S. System of Mineralogy, 6th. Edition, New York: **1892**, 427.

(8) Alexandrov, E. V.; Blatov, V. A.; Kochetkov, A. V.; Proserpio, D. M. Underlying nets in three-periodic coordination polymers: topology, taxonomy and prediction from a computer-aided analysis of the Cambridge Structural Database. *CrystEngComm* **2011**, *13*, 3947.

(9) Blatov, V. A.; O'Keeffe, M.; Proserpio, D. M. Vertex-, face-, point-, Schläfli-, and Delaney-symbols in nets, polyhedra and tilings: recommended terminology. *CrystEngComm* **2010**, *12*, 44.

(10) Blatov, V. A. Multipurpose crystallochemical analysis with the program package TOPOS. *IUCr CompComm Newsletter*. **2006**, *7*, 4.